Light propagation in stratified media with soft interfaces

N. Van den Broeck, F. Brosens, J. Tempere, and I. F. Silvera

Phys. Rev. B **93**, 155129 — Published 15 April 2016

DOI: 10.1103/PhysRevB.93.155129

Light propagation in stratified media with soft interfaces

N. Van den Broeck, F. Brosens, and J. Tempere
Theory of Quantum and Complex systems, Universiteit Antwerpen, Belgium

I.F. Silvera
Lyman Laboratory of Physics, Harvard University, Cambridge MA02138, USA
(Dated: February 16, 2016)

The propagation of light through materials in which the density of charge carriers varies smoothly on a scale smaller than or comparable to the wavelength requires a description that goes beyond the commonly used Fresnel equations. We propose a method to solve Maxwell's equations in such a way that any linear response theory for the bulk material can be combined with a given smooth density profile for the (free or bound) charge carriers. This method is implemented for linearly polarized monochromatic light impinging on inhomogeneous multilayer systems, leading to a fast algorithm that yields reflectance and transmittance for such systems. We apply our algorithm to investigate the difference in optical response between smooth interfaces and abrupt interfaces in stratified systems where the materials can have complex bulk permittivities, and find that the smoothening of the interface on a wavelength scale significantly reduces reflection in favor of absorption. This result is of importance to current experiments that aim to detect metallic hydrogen and deuterium films using their optical response. Our results show that for a correct interpretation of these experiments it is important to consider the smoothness of the density profile of the metallic layer. Also, for non-absorbing layers, a smooth, rather than abrupt transition, can have an important impact on the design of optical filters.

I. INTRODUCTION

The study of the optical properties of inhomogeneous thin films and coatings has a long history[1], and remains a very active topic of experimental and theoretical research. Practical applications are abundant and range from impedance matching[2], optical fibers[3], blu-ray players[4] to anti-reflection coatings[5,6].

When changes in the dielectric constant take place over a distance much smaller than the wavelength of the light, the Fresnel equations can be used to knit together the solutions of Maxwell's equations for neighboring layers with each layer having constant permittivity[7]. When many such layers are present, matrix methods can be successfully used to find the reflection and transmission coefficients[8]. Although most descriptions focus on non-absorbing materials, more recent work has attempted to generalize this procedure to complex permittivities[9].

Much less attention has been paid to the case when the variation of the permittivity takes place on distances smaller than or comparable to the wavelength of the light. Except for some specific profiles of the dielectric functions[10,11], analytical results are not available. Amplitude-phase methods have been put to use to tackle this problem numerically[12,13], yielding nonlinear differential equations either for the amplitude or for the phase. Thus far, these methods focus on transparent materials in order to determine and optimize reflectance properties of films and coatings[14]. Nevertheless, many systems exhibit a *complex* dielectric response varying on distances of the size of the wavelength, such as *e.g.* systems in plasma physics[15], doped semi-conductors[16] and laser-heated metals in high-pressure experiments[17]. While theories of the response of the homogeneous electron gas and other materials grow ever more detailed, the effect of smooth transitions remains insufficiently understood[18] and is neglected in most descriptions: the calculated response functions are typically used in conjunction with the approximation of an abrupt interface[19,20].

Here, we present a numerical method based on linear differential equations, to calculate efficiently the propagation of electromagnetic waves through an inhomogeneous medium with a continuous complex dielectric function that varies along the direction of propagation. We use our method to investigate inhomogeneous metal films where the electron density varies over a distance of the order of the wavelength. In particular we compare the optical response for media with inhomogeneous dielectric functions as a function of length scale to the usual approximation of a slab with a uniform dielectric function in the direction of propagation. For this purpose, we apply our method to two models: 1) a single slab with a smoothed-out interface (*e.g.* by diffusion into its environment) and 2) a model of a diamond anvil cell used in the search for metallic hydrogen, containing a position dependent mixture of molecular and metallic hydrogen.

II. METHODOLOGY

A. General formalism

Light propagation in a continuous medium is commonly described by the classical, microscopic Maxwell equations for scalar and vector potentials, where these fields are written as a sum of the externally applied fields (e.g. the incoming electromagnetic wave), and the induced fields, arising from the response of the material:

$\phi = \phi^{\text{ext}} + \phi^{\text{ind}}$ and $\mathbf{A} = \mathbf{A}^{\text{ext}} + \mathbf{A}^{\text{ind}}$. In our formalism, the inhomogeneity of the materials is incorporated at the level of the response functions *through the density of charge carriers that participate in creating the induced fields*. We write this density as $n(\mathbf{r}) = f(\mathbf{r})n_0$ where n_0 is the bulk charge carrier density. The inhomogeneity in the density is taken into account by the "profile function" $f(\mathbf{r})$.

The charge carriers can be free electrons or holes, or bound charges allowing polarization. When subject to the total fields ϕ and $\mathbf{A}$, the individual charge carriers at time t and position $\mathbf{r}$ are displaced over a distance $\mathbf{X}(\mathbf{r}, t)$. The calculation of this displacement field (not to be confused with the electric displacement field $\mathbf{D}$) is the goal of response theory. The only restriction that we impose on the choice of response theory is that the response is linear in the electric field. For monochromatic fields of frequency ω, the linearity requirement leads to

$$\mathbf{X}(\mathbf{r}, \omega) = \alpha(\omega)\mathbf{E}(\mathbf{r}, \omega), \tag{1}$$

with $\alpha(\omega)$ a (complex) proportionality constant. For example, solving the Lagrangian equation of motion of an electron using the Drude formalism for metallic materials results in

$$\alpha_{\text{Drude}} = \frac{e}{m\omega\left(\omega + i/\tau\right)}, \tag{2}$$

with m the electron mass, e its charge, and with τ the Drude relaxation time. In general, the proportionality constant α can be written in terms of the relative bulk permittivity ε_m through $en_0\alpha/\varepsilon_0 = 1 - \varepsilon_m$ with ε_0 the vacuum permittivity. Any response formalism capable of calculating ε_m can be used instead of the Drude example above.

The displacements of the charge carriers lead to a polarization field that is modulated by the profile function, $\mathbf{P}(\mathbf{r}, \omega) = -n_0 e f(\mathbf{r})\mathbf{X}(\mathbf{r}, \omega)$. Hence, the induced charge density and current can be calculated from the displacement field via

$$\rho^{\text{ind}}\left(\mathbf{r}, \omega\right) = en_0 \nabla \cdot \left[f\left(\mathbf{r}\right)\mathbf{X}\left(\mathbf{r}, \omega\right)\right], \tag{3}$$

$$\mathbf{J}^{\text{ind}}\left(\mathbf{r}, \omega\right) = i\omega n_0 f\left(\mathbf{r}\right)\mathbf{X}\left(\mathbf{r}, \omega\right). \tag{4}$$

In turn, the induced fields ϕ^{ind} and $\mathbf{A}^{\text{ind}}$ are determined by the Maxwell equations with the induced charges and currents as source terms. Eliminating the induced charges and currents from these equations yields the following differential equations:

$$\Delta\phi^{\text{ind}}\left(\mathbf{r}, \omega\right) = \varepsilon_0\left(1 - \varepsilon_m\right)\left\{\nabla f\left(\mathbf{r}\right) \cdot \left[-\nabla\phi\left(\mathbf{r}, \omega\right) + i\omega\mathbf{A}\left(\mathbf{r}, \omega\right)\right] - f\left(\mathbf{r}\right)\Delta\phi\left(\mathbf{r}, \omega\right)\right\}, \tag{5}$$

$$\left(\Delta + \frac{\omega^2}{c^2}\right)\mathbf{A}^{\text{ind}}\left(\mathbf{r}, \omega\right) = i\frac{\omega}{c^2}\left(1 - \varepsilon_m\right) f\left(\mathbf{r}\right)\left[\nabla\phi\left(\mathbf{r}, \omega\right) - i\omega\mathbf{A}\left(\mathbf{r}, \omega\right)\right] - i\frac{\omega}{c^2}\nabla\phi. \tag{6}$$

These equations are given in SI units rather than in cgs, and c is the velocity of light in vacuum. The Coulomb gauge $\nabla \cdot \mathbf{A} = 0$ has been used. Given an external perturbation (described by ϕ^{ext}, $\mathbf{A}^{\text{ext}}$) and a profile function $f(\mathbf{r})$, the solution for the induced fields ϕ^{ind}, $\mathbf{A}^{\text{ind}}$ can be found and used to calculate transmittance, reflectance, and absorptance. In the next subsection, we present a numerical scheme that solves this for a one-dimensional inhomogeneous geometry.

B. Discretization

The specific models discussed in this paper are one-dimensional, with the x-axis along the direction of the beam propagation. The incoming wave is a linearly polarized plane wave with $\phi^{\text{ext}} = 0$ and $\mathbf{A}^{\text{ext}} = \exp\left(+ikx\right)\mathbf{e}_y$.

Rewriting the differential equations (5) and (6) for this system quickly shows that the solution will have $\phi^{\text{ind}} = A_x^{\text{ind}} = A_z^{\text{ind}} = 0$, leaving only A_y^{ind} to be determined from

$$\left\{\Delta + k^2\left[1 - \left(1 - \varepsilon_m\right) f\left(x\right)\right]\right\} A_y^{\text{ind}}\left(x, \omega\right) = k^2\left(1 - \varepsilon_m\right) f\left(x\right) e^{ikx}. \tag{7}$$

Discretization on a grid using N grid points with spacing δx (a non-uniform grid is a trivial extension) yields

$$u_{j+1} = \left\{2 - \left[1 - \left(1 - \varepsilon_m\right) f_j\right] k^2 \delta x^2\right\} u_j - u_{j-1} + \left(1 - \varepsilon_m\right) f_j k^2 \delta x^2 e^{ikx_j}. \tag{8}$$

Here u_j (with $j = 1...N$) is the solution array for A_y^{ind}. The density profile at j^{th} grid point is f_j, and the position of this grid point is given by x_j.

The first and last two grid points should be situated well outside the inhomogeneous thin film. This ensures that the solution u for the induced vector potential at the first grid points describes the reflected wave. Hence, these must be of the form $u_1 = C_R$ and $u_2 = C_R \exp\left(-ik\delta x\right)$, with C_R an *a priori* unknown complex coefficient connected to the reflectance through $R = |C_R|^2$.

Having fixed the first two grid points, we obtain the entire solution array u from the recurrence relation (8) as a function of C_R. The algorithm that we propose consists in determining C_R by requiring that the induced vector potential at the last couple of grid points, at the other side of the thin film, represents a purely outgoing wave. Since at the end of the grid, the induced potential is an outgoing wave, it should not contain contributions of the form $\exp(-ikx)$, resulting in a measure

$$D(u) = |u_{N-1}\exp(ik\delta x) - u_N| \tag{9}$$

that indicates the goodness of the solution u. By minimising $D[u(C_R)]$ with respect to C_R, we obtain the reflectance. We also find the value for the induced vector potential at the last grid point, $u_N = C_T\exp(+ikx_N)$. The coefficient C_T of this outgoing wave (in combination with the external wave) determines the transmittance through $T = |1 + C_T|^2$.

C. Multiple materials

For some applications it is necessary to include multiple materials and mixtures of materials with different properties. When the overall response remains additive in the densities of charge carriers in the different materials, the extension of the formalism is straightforward. Indexing the bulk permittivities ε_m^ℓ and profile functions $f^\ell(\mathbf{r})$ for the different materials by ℓ, the solution for the induced fields can be found by simply replacing

$$(1-\varepsilon_m)f(\mathbf{r}) \to \sum_\ell (1-\varepsilon_m^\ell) f^\ell(\mathbf{r}) \tag{10}$$

in equations (5) and (6). In the discretized equation for the 1D case, this leads to

$$u_{j+1} = \left[2 - \left(1 - \sum_\ell \left(1-\varepsilon_m^\ell\right) f_j^\ell\right) k^2\delta x^2\right] u_j - u_{j-1} + \sum_\ell \left(1-\varepsilon_m^\ell\right) f_j^\ell k^2 \delta x^2 e^{ikx_j}, \tag{11}$$

where ℓ runs over the different materials. This obviously also works when the film consists of several non-overlapping materials. For mixtures, this corresponds to a weighted averaging of the ε_m^ℓ. When the bulk permittivities differ strongly, a better approximation consists in averaging the cube root of the ε_m^ℓ [21]:

$$\sum_\ell \varepsilon_m^\ell f^\ell(\mathbf{r}) \to \left(\sum_\ell f^\ell(\mathbf{r})(\varepsilon_m^\ell)^{1/3}\right)^3, \tag{12}$$

where we assume $\sum_\ell f^\ell(\mathbf{r}) = 1$.

D. Jumping over homogeneous layers

If the film contains a layer of thickness Δ through which the density of charge carriers is uniform, it is possible to speed up the implementation without loss of accuracy by incorporating the known analytic solution for the induced field in such a homogeneous layer. Setting f equal to 1, the differential equation (7) has the well known solution

$$A_y^{ind} = -e^{ikx} + c_1\cos(kx\sqrt{\varepsilon_m}) + c_2\sin(kx\sqrt{\varepsilon_m}). \tag{13}$$

Using two calculated values u_j and u_{j+1} within the layer, the unknown coefficients c_1 and c_2 can be found. Next, the analytical solution can be used to calculate $u(x_j+\Delta)$ and $u(x_j+\Delta+\delta x)$ for arbitrary large Δ, traversing slabs with constant ε_m, after which Eq. (8) can be used to resume the calculation with varying f.

III. RESULTS

A. Single soft-edged slab

Consider a slab of a material with permittivity $\varepsilon_m = -1.47 + 13.6i$ (similar to that of metallic hydrogen[20]) in a vacuum environment. The density profile of the slab is described by

$$f_{\text{slab}}(x) = \frac{1}{2}\frac{\exp\left(\frac{d}{\kappa}\right)}{\cosh\left(\frac{d}{\kappa}\right) + \cosh\left(2\frac{x-x_0}{\kappa}\right)}, \tag{14}$$

where d indicates the thickness, κ the smoothing and x_0 the position of the center of the slab. This profile is shown in inset b of Fig. 1 for $\kappa = 5$ nm and several values of d. If $\kappa \to 0$, the profile becomes a hard-wall (step) profile, and the calculation gives the same values as the analytical Fresnel equations[7] for sharp interfaces. For κ sufficiently small as compared to d the integrated value of the smooth profile is the same as that of the unit step ($\kappa = 0$), so that changing κ does not change the amount of charge carriers. However, if κ becomes too large as compared to d, the profile will no longer reach 1 in the center and the integral will diminish.

The reflectance for this system is shown in Fig. 1 as a function of the thickness for several values of κ. This clearly shows that the reflectance drops as the extent of the smoothness increases, which means that absorption must increase since the transmittance does not change. The decrease of the reflectance as a function of κ is also shown in inset a of Fig. 1, which clearly shows that for very large κ the reflectance can differ substantially from the bulk reflectance and even go to zero meaning that almost all the energy is absorbed.

Fig. 1 also demonstrates the behaviour of the optical properties of slabs as their dimensions become smaller. For a thick slab, transmission is zero and the reflectance is constant for thicknesses greater than a certain value,

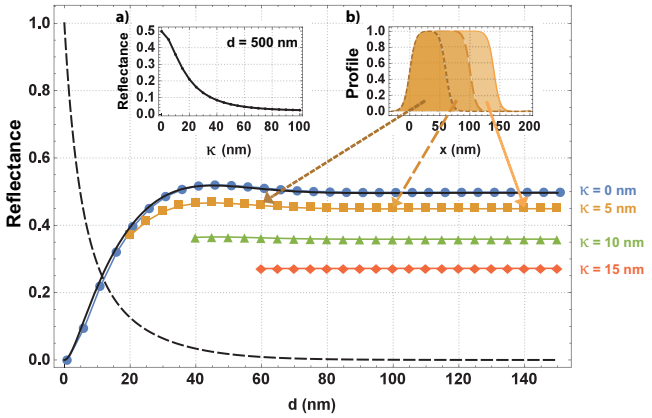

Figure 1. Reflectance of a slab with $\varepsilon_m = -1.47 + 13.6i$, as a function of thickness d and for various values of κ: 0 nm (disks), 5 nm (squares), 10 nm (triangles) and 15 nm (diamonds). The solid line represents the analytical result for a sharp edged profile. The dashed line on the main figure shows the transmittance which is not affected by changing κ. Inset a) shows the reflectance of a large 500 nm thick slab as a function of κ. Inset b) demonstrates three profiles with $\kappa = 5$ nm but different thicknesses. The reflectance of these profiles are indicated by the arrows. These calculations have been performed with $\lambda = 500$ nm.

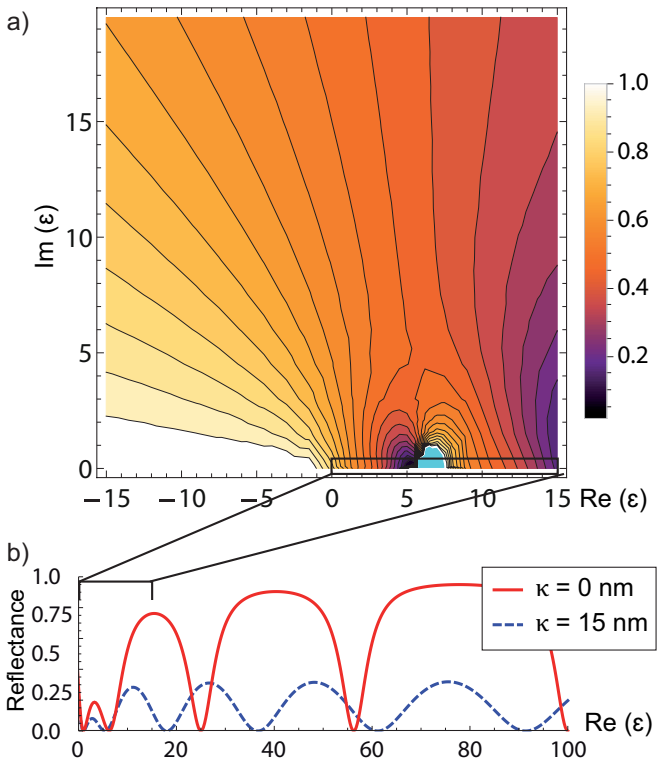

Figure 2. a) Contour plot showing the ratio between the reflectance calculated with $\kappa = 15$ nm and $\kappa = 0$ nm for different permittivities and for $d = 100$ nm. Light colors mean almost no difference, dark colors means the reflectance drops for larger κ. b) Reflectance for $\kappa = 15$ nm (dashed) and $\kappa = 0$ (solid) for positive permittivities with negligible imaginary part. Calculations are performed for $\lambda = 500$ nm.

which is about 60 nm for an abrupt interface ($\kappa = 0$) in the case shown in Fig. 1. However the value of the thick film reflectance depends on κ, and the threshold for the changeover to thin film reflectance is lowered if the profile is smoother (κ larger).

The change in reflectance is also dependent on the bulk permittivity of the material as demonstrated in Fig. 2a, which shows the ratio between the reflectance for $\kappa = 15$ nm and $\kappa = 0$ nm for different bulk permittivities and for a film of thickness 100 nm. Negative but real bulk permittivities show no difference in reflectance between the sharp and smoothed profiles. The largest difference occurs for positive permittivities, where oscillations occur due to interference between multiple reflections in the film. Figure 2b shows the reflectance for both profiles in this oscillatory region. Smoothing the profile changes how well the light fits in the cavity and thus the constructive or destructive nature of the interference. In this case the influence of the profile is largest and reflectance can be both promoted and suppressed.

B. Multilayer films

As a second example of this algorithm we present a model inspired by the recent search for metallic hydrogen[22] at static pressures using a diamond anvil cell with pulsed laser heating and metallic deuterium[23] using programmed shock compression. The transition from molecular to metallic hydrogen is accompanied by a change in the optical properties, notably an abrupt change in reflectance and transmittance when a phase line is crossed from liquid molecular to atomic metallic hydrogen. The sudden change in optical properties is used to experimentally characterize the transition. In the laser heated diamond anvil cell the thickness of the metallic film varies from a few nm to $\sim$ 50-100 nm depending on the temperature, and the reflectance increases to a thick film saturation value of ~ 0.55. Since this is the value expected for bulk metallic hydrogen our analysis implies that the electron density of the film rapidly rises and the there is little smoothing, so the profile must be that of a sharp block, according to Fig. 1.

The shocked deuterium sample is much thicker, about 10 microns, and at the end of the ramp is expected to be completely transformed to a metallic liquid. A monochromatic beam of light passes through the deuterium and reflects back off of an Al surface; when the deuterium is metallic the reflectance of the beam is about 0.45. However during the ramp up in pressure and temperature, the reflected beam is strongly attenuated and then recovers to reach 0.45. This attenuation was interpreted as being due to interband transitions of the molecular deuterium. However, the spectrum was not measured, to confirm this. The authors state that during the compression to the metallic state there is probably spatial heterogeneity in the density. Using our analysis, an alternate explanation is that during the formation of

the thick metallic film an inhomogeneous liquid metal develops with a large value of κ as in Fig. 1, so that the reflectance approaches zero and recovers as the inhomogeneity collapses into a uniform slab of metal.

Modeling the diamond anvil cell setup requires including several layers of materials and a mixture of molecular and metallic hydrogen. A tungsten film is present as a heating source for the experiment, and is separated from the hydrogen by a transparent cladding layer for which we assume vacuum permittivity. The materials used in the calculations are tungsten with $\varepsilon_{\rm W} = 4.28 + 18.3i$[25], molecular hydrogen with $\varepsilon_{\rm H_2} = 6.27$[26] (calculated for 150 GPa) and metallic hydrogen with $\varepsilon_{\rm MH} = -1.47 + 13.6i$[20]. All calculations are preformed with $\lambda = 500$ nm. The thickness of the tungsten film, as reported in the experiment[22], is $\sim$ 8.5 nm. The experiment also characterized the optical properties of the tungsten film approximately: R=0.25, T=0.25 and A=0.5. Using the algorithm presented here, we find that these optical properties are achieved for a tungsten film with a thickness of 8.8 nm, in accordance with the reported thickness. An additional layer of vacuum is added on the left hand side of the grid in order to place u_1, u_2, u_{N-1} and u_N outside the stack of films as required by our algorithm. The resulting DAC forms a cavity mode, so that the results are sensitive to how well standing waves fit in between its edges. In order to mitigate this effect the results shown are averages over DAC widths within a wavelength interval.

As the exact density profile of the metallic hydrogen film is not known, we compare two extreme cases: (1) a sharp-edged block and (2) an exponential decay away from the heater and into the molecular hydrogen. The profile functions for the two cases are illustrated in the insets of figure 3, where the dot-dashed curves represent the profile for the tungsten, the full curve that for metallic hydrogen, and the dashed line that of molecular hydrogen.

In figure 3 we show the results for the reflectance $R(d)$ and transmittance $T(d)$ as a function of the thickness d of the layer. Both quantities are normalized by their value (due to the tungsten film) at $d = 0$, when no metallic hydrogen is present. The presence of the metallic hydrogen increases the reflectance (upper two curves, red), and decreases the transmittance (lower two curves, blue). To compare the sharp-edged block (dashed curves) with the exponentially decaying profile (full curves), we choose a decay length such that the integrated density of the MH is the same in both cases. In agreement with the results from the previous subsection, we find that smoothing the profile reduces reflectance and, to a lesser extent, also transmittance. Note that for the smoothed metallic hydrogen our formalism enables us to take into account the molecular hydrogen at the smoothed interface.

The true density profile of the layer of metallic hydrogen is unknown, and will depend on the specific experimental procedure followed. It is likely to be in between the extremes of a hard wall and an exponential smooth

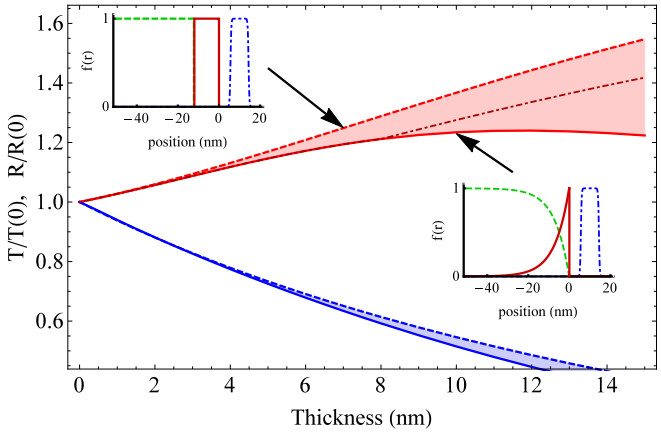

Figure 3. (color online) The upper two curves show the reflectance $R(d)$, normalized to $R(0)$, as a function of the thickness d of the metallic hydrogen film, for (1) a smooth, exponential density profile (full curve) and (2) a hard-wall profile (dashed curve). These profiles are shown in the inset (full curves), along with the profile for the tungsten heating layer (dash-dotted curve) and the molecular hydrogen (dashed curve). The lower two curves show the same results, but for the transmittance $T(d)$, again normalized to $T(0)$. The dash-dotted line shows the result for the intermediate case of a layer that first grows with a smooth profile until it reaches 8 nm, and then thickens by growing a uniform metallic hydrogen layer.

profile. Hence, the true reflectance and transmittance are expected to lie in between the dashed curves and the full curves. This region (shaded in figure 3) indicates the uncertainty stemming from not knowing the true density profile of the film of metallic hydrogen. The dash-dotted curve in Fig. 3 shows an "intermediate" case, lying in this region. It represents a layer that starts to grow as a smooth interface between metallic and molecular hydrogen, until this interface reaches 8 nm thickness. Then it continues to grow by adding a uniform density layer of metallic hydrogen behind the smooth interface. This appears to describe the profile of the experimentally produced metallic hydrogen for which the reflectance rises to the expected bulk value for thicker films.

Several recent papers have made improvements in the calculation of the dielectric function for bulk metallic hydrogen[19,20], and relate these results to the reflectance and transmittance via the Fresnel equations for abrupt interfaces. However, the present results indicate that the experimental verification of these improvements in the response theory of metallic hydrogen will require a more careful analysis of the density profile.

IV. CONCLUSIONS

By separating the density profile from the bulk properties of materials we have derived general differential equations for the optical response of a system with smoothly

varying density profiles, and we have proposed a numerical discretization and minimization algorithm to solve these equations in a one-dimensional system. The resulting algorithm is fast, easy to implement and powerful, capable of handling large systems, multiple materials with arbitrary density profiles and even mixtures of materials.

Using the algorithm, we find that there is a significant difference in response between a layer with abrupt interface and a layer with smoothly varying charge carrier density. Qualitatively, the reflectance is lowered in favor of the absorption when smoothing the transition between two layers, one of which has complex bulk permittivity. Interfaces with large smoothing can completely suppress reflection, which can be of use for creating high-absorbing structures. A very strong impact is also found for materials with permittivities with positive real part and negligible imaginary part. The optical response of films of such materials are already dependent on the distance between their interfaces, as in a Fabry–Pérot interferometer. Smoothing the edges directly impacts the interference between the interfaces.

Finally, we note that the results presented here are of importance to the interpretation of ongoing experiments searching for the transition between molecular and metallic hydrogen by detecting a change in the optical properties. These experiments produce metallic hydrogen by pulsed laser heating, which is not expected to create a uniform slab with an abrupt interface. We estimate that discrepancies as large as 10% in reflectance can be expected when assuming an abrupt interface. Many more applications of this algorithm can be conceived, *e.g.* in the area of plasmas where the density is important and may vary spatially, in semiconductors where doping alters the density or when pn-junctions are created, and for systems with negative refractive index materials. The algorithm presented here opens a new way of investigating the optical properties of smoothly varying density profiles on a nanoscopic scale.

ACKNOWLEDGMENTS

The authors would like to thank M. Zaghoo, and A. Salamat for discussions and suggestions. This research was funded by a Ph.D. grant of the Agency for Innovation by Science and Technology (IWT). This research was also supported by the Flemish Research Foundation (FWO-Vl), project nrs. G.0115.12N, G.0119.12N, G.0122.12N, G.0429.15N and by the Scientific Research Network of the Research Foundation-Flanders, WO.033.09N. The research was supported by the NSF, grant DMR-1308641, and by the DOE Stockpile Stewardship Academic Alliance Program, grant DE-NA0001990.

[1] J.R. Jacobsson, *"Review of the optical properties of inhomogeneous thin films"*, in J.A. Dobrowolski, P.G. Verly, Proc. SPIE 2046 (Eds.), *Inhomogeneous and quasi-inhomogeneous optical coatings*, vol.2, SPIE, Quebec City, Canada (1993).

[2] J. Kröll, J. Darmo, and K. Unterrainer, Opt. Express **15**, 6552 (2007).

[3] M. D. Feit and J. A. Fleck, Applied Optics **17**, 3990-3998 (1978).

[4] K.-Y. Hung and J.-C. Liao, J. Micromech. Microeng. **18**. 075022 (2008).

[5] A. Mahdjoub, L. Zighed, Thin Solid Films **478**, 299 (2005).

[6] A. Thoman, A. Kern, H. Helm, and M. Walther, Phys. Rev. B **77**, 195405 (2008).

[7] E. Hecht, *Optics* (4th edn., Addison-Wesley, 1998).

[8] F. Abeles, Ann. Phys. Fr. **5**, 706-784 (1950).

[9] J.I. Larruquert, J. Opt. Soc. Am. A **23**, 99-107 (2006).

[10] P.S. Epstein, Proc. Nat. Acad. Sci. **16**, 627-637 (1930).

[11] S.H. Mazharimousavia, A. Roozbeh and M. Halilsoy, J. Electromagn. Waves Appl. **27**, 2065 (2013).

[12] M. Fernandez-Guasti, A. G.Villegas and R. Diamant, Rev. Mex. Fis. **46**, 530 (2000).

[13] R. Diamant and M. Fernandez-Guasti, J. Opt. A: Pure Appl. Opt. **11**, 045712 (2009).

[14] R. Diamant and M. Fernandez-Guasti, Optics Comm. **294**, 64-72 (2013).

[15] Y. Qiu, H. Guo, M. Liu, H. Tang, D. Deng, and H.J. Kong, Journ. Korean Phys. Soc. **41**, 722-725 (2002).

[16] G. Malpuech, A. Kavokin, and G. Panzarini, Phys. Rev. B **60**, 16788 (1999).

[17] S. Deemyad, E. Sterer, C. Barthel,S. Rekhi, J. Tempere, I.F. Silvera, Rev. Sci. Instrum. **76**, 125104 (2005).

[18] G. Toscano, J. Straubel, A. Kwiatkowski, C. Rockstuhl, F. Evers, H. Xu, N.A. Mortensen and M. Wubs, Nat. Comm. **6**, 7132 (2015).

[19] B. Holst, R. Redmer, and M.P. Desjarlais, Phys. Rev. B **77**, 184201 (2008).

[20] L. A. Collins, S. R. Bickham, J. D. Kress, S. Mazevet, T. J. Lenosky, N. J. Troullier, and W. Windl, Phys. Rev. B **63**, 184110 (2001).

[21] Landau L.D. and Lifshitz E.M., *Electrodynamics of continuous media, Ed. 2* (Pergamon press), 1984, pp. 42-43.

[22] M. Zaghoo, A. Salamat and I.F. Silvera, arXiv:1504.00259 .

[23] M.D. Knudson, M.P. Desjarlais, A. Becker,R.W. Lemke, K.R. Cochrane, M.E. Savage, D.E. Bliss, T.R. Mattsson, R. Redmer, Science 348, 1455-1460 (2015)

[24] S. Rekhi, J. Tempere, I.F. Silvera, Ref. Sci. Instrum. **74**, 3820-3825 (2003).

[25] Lide D.R., *CRC handbook of Chemistry and Physics* (CRC Press) 2005, pp. 12/153.

[26] W.J. Evans and I.F. Silvera, Phys. Rev. B **57**, 14105 (1998).